Ethylene Insertion in the Homogenous Ziegler–Natta Catalysis: An ab Initio Investigation on a Correlated Level

Horst Weiss, Michael Ehrig, and Reinhart Ahlrichs*

Contribution from the Institut für Physikalische Chemie und Elektrochemie, Lehrstuhl für Theoretische Chemie, Universität Karlsruhe, Kaiserstrasse 12, 76128 Karlsruhe, Germany

Received September 9, 1993. Revised Manuscript Received March 7, 1994®

Abstract: The first ab initio investigation of a realistic Ziegler–Natta system is presented that includes dynamical electron correlation to determine more reliable geometries and energetics during the ethylene insertion process. The systems $Cp_2TiCH_3^+$–C_2H_4 and $Cl_2TiCH_3^+$–C_2H_4 were investigated with the Møller–Plesset second-order perturbation method and the local density functional method. The quality of the MP2 energetics has been checked through single point coupled cluster singles doubles (triples) calculations for the $Cl_2TiCH_3^+$–C_2H_4 system. The results strongly support the mechanism proposed by Brookhart and Green. Agostic interactions were found to be of crucial importance. Two basic concepts of the Cossee–Arlman mechanism could not be confirmed: neither a precoordinated monomer nor a transition state was found to be a critical point on the potential energy surface for $Cp_2TiCH_3^+$–C_2H_4. The educt $Cp_2TiCH_3^+$ has carbenoid character. The ethylene insertion is then rationalized by reference to a 2 + 2 addition which is symmetry allowed through the availability of d orbitals.

I. Introduction

Various attempts have been made to rationalize the mechanism of the Ziegler–Natta catalysis.[1] We concentrate here on the soluble two-component ethylene polymerization catalytic system Cp_2TiCl_2–$RAlCl_2$, since experiments[2-4] have in principle clarified the sequence of reactions from the formation of the active catalyst to the ethylene insertion into the Ti–C bond. Following the arguments of Eisch and co-workers,[2] we consider the following sequence of reactions as well established:

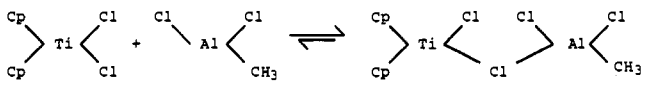

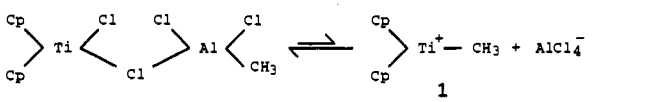

1

This mechanism implies that the active catalyst **1** is formed in two successive equilibria. This is consistent with the kinetic studies of Fink and Zoller.[3] The ion-pair nature of the active catalyst **1** has recently been proven in a direct way first by Yang, Stern, and Marks[5] for zirconocenes and by Eisch and co-workers[6] for titanocenes. Eisch et al. treated ((trimethylsilyl)methyl)titanocene dichloride with the Lewis acid $AlCl_3$ and obtained (via NMR spectroscopy) direct evidence for the heterolysis of the Ti–Cl bond and the formation of the ion-pair $Cp_2Ti^+CH_2$–$SiMe_3$–$AlCl_4^-$.

The following crucial step of the Ziegler–Natta catalysis, the ethylene insertion, is far less known. Although Eisch and co-workers[2] succeeded in isolating the intermediate of the insertion, there is no information about what happens on the molecular level when the ethylene monomer enters the sphere of the active catalyst **1**. Several mechanisms for the ethylene insertion have been considered.

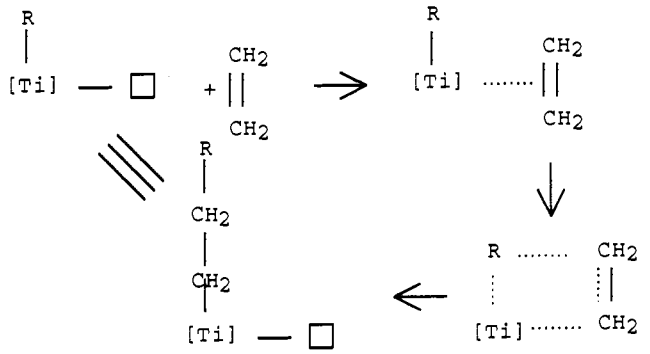

Figure 1. Cossee–Arlman mechanism.

The traditional mechanism, proposed by Cossee and Arlman[7] (Figure 1), starts from the precoordination of the monomer at a free site of the active catalyst, leading to the formation of a π complex similar to, for example, Zeise's olefinic complex. In the following step, a simple alkyl migration to the complex-bound monomer should occur to form the new carbon–carbon bond. The intermediate or the transition state is assumed to be a four-membered ring of Ti, the α-carbon atom of the growing polymer chain, and the two carbon atoms of the monomer. This mechanism (outlined in Figure 1) is widely accepted, but one should bear in mind that there is no empirical evidence for the existence of the precoordinated monomer. On the contrary, Fink and Rottler[4] in their NMR studies have stressed that there are no spectroscopical hints for the existence of a precoordinated monomer. Furthermore, there are no experiments that have given evidence for the four-membered transition state as a saddle point of the energy hypersurface.

An accepted alternative to the Cossee–Arlman mechanism has been worked out by Brookhart and Green.[8] It is sketched in Figure 2. According to this mechanism, the formation of the carbon–carbon bond is assisted by strong α-agostic interactions between the unsaturated metal center (Ti, Zr, etc.) and the α-C–H

* Abstract published in *Advance ACS Abstracts*, May 1, 1994.

(1) For general information: Boor, J., Jr. *Ziegler-Natta Catalysts and Polymerization*; Academic Press: New York, 1979. For later work see refs 2 and 5 given in: Kawamura-Kuribayashi, H.; Koga, N.; Morokuma, K. *J. Am. Chem. Soc.* **1992**, *114*, 8687.

(2) Eisch, J. J.; Piotrowski, A. M.; Brownstein, S. K.; Gabe, E. J.; Lee, F. L. *J. Am. Chem. Soc.* **1985**, *107*, 7219.

(3) Fink, G.; Zoller, W. *Makromol. Chem.* **1981**, *182*, 3265.

(4) Fink, G.; Rottler, R. *Angew. Makromol. Chem.* **1984**, *94*, 25.

(5) Yang, X.; Stern, C. L.; Marks, T. J. *J. Am. Chem. Soc.* **1991**, *113*, 3623.

(6) Eisch, J. J.; Caldwell, K. R.; Werner, S.; Krüger, C. *Organometallics* **1991**, *10*, 3417.

(7) (a) Cossee, P. *J. Catal.* **1964**, *3*, 80. (b) Arlman, E. *J. Catal.* **1964**, *3*, 80. (c) Arlman, E. J.; Cossee, P. *J. Catal.* **1964**, *3*, 99.

(8) Brookhart, M.; Green, M. L. H. *J. Organomet. Chem.* **1983**, *250*, 395.

0002-7863/94/1516-4919$04.50/0

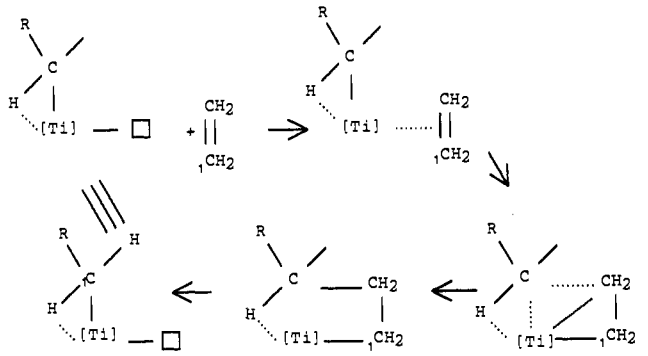

Figure 2. Brookhart–Green mechanism.

bond of the growing polymer chain. Initially, a metallacycle intermediate is formed. The polymerization proceeds with the isomerization of the γ-agostic metallacycle intermediate to the product of the monomer insertion with an α-C–H–Ti bond. It should be noted that no H/D isotope effects have been observed by Soto, Steigerwald, and Grubbs[9] in a time determining step. Therefore no hydrogen migration occurs, which is consistent with the model of agostic interactions.

One would expect that ab initio calculations would provide answers to the questions of structure and mechanism just discussed. Since this reaction involves a transition metal as the reactive center, it is necessary to include electron correlation. The calculations published so far[10-15] had to resort to noncorrelated methods for geometry optimizations because of computational limitations. Correlation effects were accounted for by single point second-order Møller–Plesset perturbation (MP2)[16] calculations for semiempirical[11] or SCF[12]-optimized geometries. Recently, highly correlated single point MCPF[17] (modified coupled pair functional) calculations for model systems involving second-row transition metals at their SCF equilibrium geometries have been performed by Siegbahn.[15] Siegbahn has argued that, for second-row transition metal compounds, it is reasonable to determine the energetics at SCF-optimized geometries since calculations on similar model systems had shown that SCF- and MCPF-optimized geometries give very similar relative energies. We agree that second-row transition metals are by far less critical than their first-row analogues. For the actual systems under consideration involving titanium, our results show (see e.g. Table 1) that the inclusion of electron correlation is necessary for the determination of the equilibrium geometries. SCF-optimized geometries are not appropriate in our cases.

The progress made in the implementation of direct MP2 gradients[18] now allows for the geometry optimization of systems occurring in the homogenous Ziegler–Natta catalysis and of systems of comparable size in general. Besides that, with the local density functional (LDF),[19] a method is now at hand that combines the consideration of dynamical electron correlation with computational costs comparable to the SCF method. However, presently, there is not sufficient experience available with this method that would allow for predictions of the reliability of the results obtained solely by applications of LDF.

We therefore decided to use SCF, MP2, and also LDF for our investigations to allow for comparisons. As far as possible, i.e. as long as computational facilities available to us permitted, the MP2 results have been checked by single point CCSD(T) (coupled cluster singles and doubles (triples))[20] calculations. The mechanism of the olefin insertion is investigated for two systems: The first system, $Cl_2TiCH_3^+$–C_2H_4, has model character since it does not polymerize ethylene but allows olefin insertion. It has been investigated by several authors,[11,12] but optimized geometries on a correlated level have not been reported. The second system, $Cp_2TiCH_3^+$–C_2H_4, is an active catalyst.[21] We present our SCF, MP2, and LDF results that give new results and insights, as will be reported in section IV. We demonstrate that inclusion of dynamical electron correlation is necessary even to get a qualitatively correct picture of the ethylene insertion.

Table 1. Comparison of Methods: The Energetics of the Ethylene Insertion in the $Cp_2TiCH_3^+$–C_2H_4 System on Various Levels of Theory[a]

	SCF/SCF,[b] E_{rel} (kJ/mol)	MP2/SCF,[c] E_{rel} (kJ/mol)	MP2/MP2,[d] E_{rel} (kJ/mol)	LDF, E_{rel} (kJ/mol)
π complex	−22.3	−99.0	*e*	*e*
transition state	52.2	−121.7	*e*	*e*
γ-agostic product	−90.9	−135.2	−188.9	−195.1
α-agostic product			−142.2	−193.8
β-agostic product			−197.9	−211.6

[a] The energy is given relative to $Cp_2TiCH_3^+$ and C_2H_4 in kJ/mol. [b] SCF energy at the SCF equilibrium geometry, basis B. [c] MP2 energy at the SCF equilibrium geometry, basis B. [d] MP2 energy at the MP2 equilibrium geometry, basis B. [e] Does not exist on the correlated level.

II. Methods of Computation

SCF and MP2 geometry optimizations have been performed with the program system TURBOMOLE.[22] LDF energy and gradient calculations were carried out with DMol.[23] The Hedin–Lundquist[24] local correlation functional has been used throughout. A gradient correction has not been applied. To check the energetics of the MP2 method, single point CCSD(T)[20] calculations at the MP2 equilibrium geometries have been performed for the system $Cl_2TiCH_3^+$–C_2H_4 by employing the program system ACES II.[25] For the geometry optimization and the saddle point search, the program Relax of the TURBOMOLE package has been used throughout, also for the optimizations based on the LDF method. No local symmetry has been assumed and no symmetry constraints have been imposed in any optimization. The validity of the Hartree–Fock picture has been checked by means of SCF instability calculations[26] with the TURBOMOLE module Escf.[27]

For the LDF calculations, a basis set of DND[23] (double-numerical+d) quality (which is comparable to a Gaussian 6-31G* basis set) has been used. Three different basis sets A, B, and C for Ti were employed in the SCF and MP2 calculations: A, SV (split valence) (14s8p5d)/[5s2p2d][28]+1p(0.05); B, as A but 2p-

(9) Soto, J.; Steigerwald, M. L.; Grubbs, R. H. *J. Am. Chem. Soc.* **1982**, *104*, 4479.
(10) Fujimoto, H.; Yamasaki, T.; Mizutani, H.; Koga, N. *J. Am. Chem. Soc.* **1985**, *107*, 6157.
(11) Jolly, C. A.; Marynick, D. S. *J. Am. Chem. Soc.* **1989**, *111*, 7968.
(12) Kawamura-Kuribayashi, H.; Koga, N.; Morokuma, K. *J. Am. Chem. Soc.* **1992**, *114*, 2359.
(13) Kawamura-Kuribayashi, H.; Koga, N.; Morokuma, K. *J. Am. Chem. Soc.* **1992**, *114*, 8687.
(14) Koga, N.; Morokuma, K. *Chem. Rev.* **1991**, *91*, 823.
(15) Siegbahn, P. E. M. *Chem. Phys. Lett.* **1993**, *205*, 290.
(16) Møller, C.; Plesset, M. S. *Phys. Rev.* **1934**, *46*, 618.
(17) Ahlrichs, R.; Scharf, P.; Ehrhardt, C. *J. Chem. Phys.* **1985**, *82*, 890.
(18) (a) Pople, J. A.; Krishnan, R.; Schlegel, H. B.; Binkley, J. S. *Int. J. Quantum Chem., Symp.* **1979**, *13*, 225. (b) Frisch, M. J.; Head-Gordon, M.; Pople, J. A. *Chem. Phys. Lett.* **1990**, *166*, 275. (c) Frisch, M. J.; Head-Gordon, M.; Pople, J. A. *Chem. Phys. Lett.* **1990**, *166*, 281. (d) Haase, F.; Ahlrichs, R. *J. Comput. Chem.* **1993**, *14*, 907.
(19) (a) Hohenberg, P.; Kohn, W. *Phys. Rev. B* **1964**, *136*, 864. (b) Kohn, W.; Sham, L. J. *Phys. Rev. A* **1965**, *140*, 1133.
(20) (a) Purvis, G. D.; Bartlett, R. J. *J. Chem. Phys.* **1982**, *76*, 1910. (b) Raghavachori, K.; Trucks, G. W.; Pople, J. A.; Head-Gordon, M. *Chem. Phys. Lett.* **1989**, *157*, 479.
(21) Taube, R.; Krukowska, L. *J. Organomet. Chem.* **1988**, *347*, C9.
(22) Ahlrichs, R.; Bär, M.; Häser, M.; Horn, H.; Kölmel, C. *Chem. Phys. Lett.* **1989**, *162*, 165.
(23) (a) Delley, B. *J. Chem. Phys.* **1990**, *92*, 508. (b) *DMol User Guide*; BIOSYM Technologies: San Diego, CA, 1993.
(24) Hedin, L.; Lundqvist, B. I. *J. Phys. C* **1971**, *4*, 2064.
(25) Stanton, J. F.; Gauss, J.; Watts, J. D.; Lauderdale, W. J.; Bartlett, R. J. *Int. J. Quant. Chem., Symp.* **1992**, *26*, 879.
(26) Chambaud, G.; Levy, B.; Millie, P. *Theor. Chim. Acta* **1978**, *48*, 103.
(27) Weiss, H.; Ahlrichs, R.; Häser, M. *J. Chem. Phys.* **1993**, *99*, 1262.
(28) Schäfer, A.; Horn, H.; Ahlrichs, R. *J. Chem. Phys.* **1992**, *97*, 2571.

Table 2. Three Lowest Eigenvalues of the HF Singlet, Triplet, and Nonreal Instability Matrices of the Educt ($Cp_2TiCH_3^+$), γ-Agostic Product, π Complex, and TS (transition state), Basis B and SCF Equilibrium Geometry

type	$Cp_2TiCH_3^+$	π complex	TS	γ-agostic product
singlet	0.114	0.116	0.119	0.107
	0.120	0.130	0.133	0.109
	0.132	0.136	0.142	0.125
triplet	−0.021	−0.027	−0.032	−0.042
	0.051	0.024	0.059	0.051
	0.053	0.048	0.060	0.052
nonreal	0.096	0.101	0.109	0.083
	0.108	0.127	0.127	0.094
	0.137	0.127	0.132	0.121

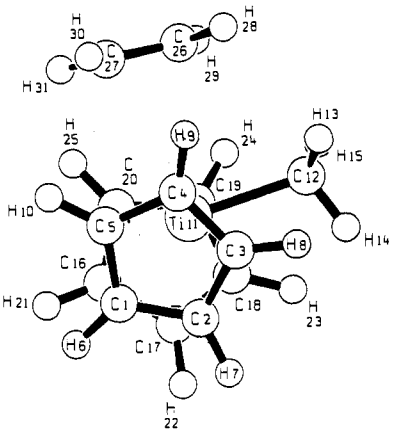

Figure 3. Optimized geometry of the precoordinated ethylene (π complex) on $Cp_2TiCH_3^+$ at the SCF level, basis B as described in section II. Important bond distances (pm) and angles (deg) are as follows: Ti11–C12, 213; Ti11–C26, 297; Ti11–C27, 304; Ti11–H14, 269; C12–H14, 110; C12–H13, H15, 109; C12–C26, 314; C27–C26, 134; C26–H28, H29, 109; C27–H30, H31, 109; C–C(Cp), 141–142; Ti11–center(Cp), 209/210; Ti11–C(Cp), 238–245; center(Cp)–Ti–center(Cp), 135.1; Ti11–C12–H13, 111.7; Ti11–C12–H14, 108.5; Ti11–C12–H15, 111.3; H30–C27–H31, 116.3; H29–C26–H28, 116.6; dihedral H21–C16–C1–H6, 26.0; dihedral C27–C26–C12–Ti11, 18.0; out-of-plane bend H28–H29–C27–C26, 4.7; out-of-plane bend H31–H30–C26–C27, 5.2.

(0.101561, 0.034054);[29] C, (14s9p5d)/[8s5p3d][29]+2p(0.101561, 0.034054). Bases A and B differ only in their polarization functions. They are based on a (14s8p5d)/[5s2p2d]SV basis set.[28] In basis A, one diffuse p function with exponent 0.05 was added. For basis B, the two 4p functions recommended by Wachters[29] with exponents 0.101561 and 0.034054 were chosen. Basis C served as a reference. Starting from Wachters (14s9p5d)/[8s5p3d] basis set, both exponents and contraction coefficients were reoptimized.[28] Finally, Wachters two 4p 0.101561 and 0.034054 functions were added to yield basis C. Within basis B (193 basis functions in C_1 symmetry), one MP2 gradient calculation took 19 h of wall clock time on a HP 735 workstation with disk storage requirements of roughly 1.5 Gbyte; a complete optimization cycle took 20–21 h.

The basis sets for all other elements were chosen as follows: Cp ring carbons, throughout (7s4p)/[3s2p]SV;[28] C_2H_4 and CH_3 carbons, throughout (7s4p)/[3s2p]SV[28]+1d(0.6);[30] hydrogen, (4s)/[2s]SV[28] throughout; chlorine, (10s7p)/[4s3p]SV[28]+1d(0.514).[30]

III. Results of the SCF Instability Analysis

The treatment of transition metal compounds is complicated through correlation effects due to partially filled d orbitals which deserve special considerations. In the cases considered here, we have only formal d^0 systems and these behave almost like main row elements. To give an example, equilibrium distances obtained on the SCF level are much more reliable than for d^n systems like ferrocene. The present basis A leads to an equilibrium distance for $TiCl_4$ of 216.3 pm, just 2.7 pm shorter than the experimental value.[31] Even equilibrium distances for V^v complexes behave in a similar way.[32] It may thus be expected that MP2 does rectify the remaining errors of the SCF approximation to a large extent.

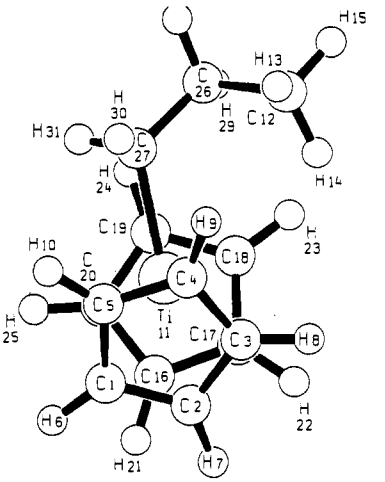

Figure 4. Optimized geometry of the γ-agostic propyl complex, the primary ethylene insertion product into the Ti–C bond of $Cp_2TiCH_3^+$ at the SCF level, basis B as described in section II. Important bond distances (pm) and angles (deg) are as follows: Ti11–C12, 360; Ti11–C27, 214; Ti11–H14, 318; C12–C26, 153; C27–C26, 154; C12–H14, 110; C12–H13, H15, 110; C27–H30, H31, 109; C–C(Cp), 141–142; Ti11–center(Cp), 207/207; Ti11–C(Cp), 239–241; center(Cp)–Ti–Center(Cp), 139.4; Ti11–C12–H14, 59.0; Ti11–C27–C26, 118.1; C27–C26–C12, 114.1; C26–C12–H14, 112.2; C12–H14–Ti11, 103.8; H14–Ti11–C27, 62.1; out-of-plane bend H31–Ti11–H30–C27, 64.3; out-of-plane bend H30–H31–Ti11–C27, 61.0; dihedral H21–C16–C1–H6, −41.5; dihedral C27–C26–C12–H14, 62.3.

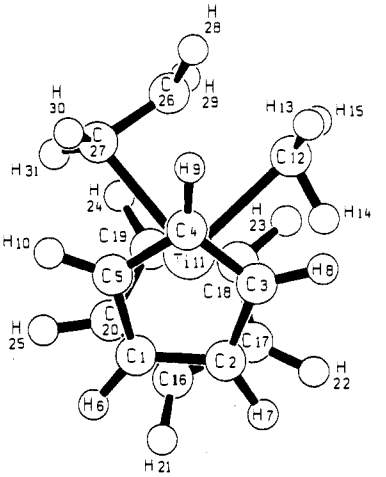

Figure 5. SCF transition state of the ethylene insertion into the Ti–C bond of $Cp_2TiCH_3^+$, basis B as described in section II. Important bond distances (pm) and angles (deg) are as follows: C12–C26, 219; Ti11–C12, 222; Ti11–C26, 256; Ti11–C27, 228; Ti11–H14, 219; C12–H14, 111; C12–H13, H15, 109; C27–C26, 140; C26–H28, H29, 108; C27–H30, H31, 108; C–C(Cp), 141–143; Ti11–center(Cp), 211/212; Ti11–C(Cp), 241–246; center(Cp)–Ti–center(Cp), 133.7; Ti11–C12–H13, 119.0; Ti11–C12–H14, 73.9; Ti11–C12–H15, 128.4; H30–C27–H31, 114.4; H29–C26–H28, 115.0; dihedral H21–C16–C1–H6, −38.9; dihedral C27–C26–C12–Ti11, 12.8; out-of-plane bend H28–H29–C27–C26, 22.7; out-of-plane bend H31–H30–C26–C27, 32.2; H13–H15–Ti11–C12, 22.7; H15–Ti11–H13–C12, 14.7.

(29) Wachters, A. J. H. *J. Chem. Phys.* **1970**, *52*, 1033.
(30) Huzinaga, S. *Gaussian basis sets for molecular calculations*; Physical Sciences Data 16; Elsevier: Amsterdam, 1984.
(31) Wells, A. F. *Structural inorganic chemistry*, 5th ed.; Clarendon Press: Oxford, U.K., 1984.
(32) Ehrig, M.; Ahlrichs, R. *Theor. Chim. Acta* **1992**, *81*, 245.

Table 3. The Ethylene Insertion Step by Step: MP2 Energies along the Reaction Path[a]

d(C12–C26) (pm)	E_{MP2} (hartree)	E_{rel} (kJ/mol)	intern. grad.[b]
∞	−1 351.198 507	0.0	0
270	−1 351.235 712	−97.70	0.003 3
258	−1 351.236 465	−99.68	0.002 4
248	−1 351.236 828	−100.63	0.001 6
245.9	−1 351.236 902	−100.83	0.000 9
243	−1 351.236 968	−101.00	0.001 4
238	−1 351.237 100	−101.35	0.001 4
233	−1 351.237 244	−101.72	0.001 8
228	−1 351.237 435	−102.22	0.002 5
223	−1 351.237 713	−102.95	0.003 8
218	−1 351.238 132	−104.06	0.006 1
213	−1 351.238 495	−105.01	0.010 6
208	−1 351.239 683	−108.13	0.014 5
185	−1 351.251 172	−138.30	0.035 8
158, γ-agostic product	−1 351.265 188	−175.10	<threshold[c]

[a] As already explained in the text, neither a π complex nor a saddle point could be located. The insertion is spontaneous for the system investigated here. The reaction path was obtained by MP2 gradient optimizations at fixed distances for the carbon atoms forming the new bond. Basis A was used throughout. [b] Internal gradients of the fixed carbon–carbon stretch. Although the gradients became very small around 245 pm, they never vanished even when a saddle point searcher was applied without fixing a coordinate. The energy surface appears to be extremely flat. Units are hartree/bohr. [c] 10^{-3} hartree/bohr.

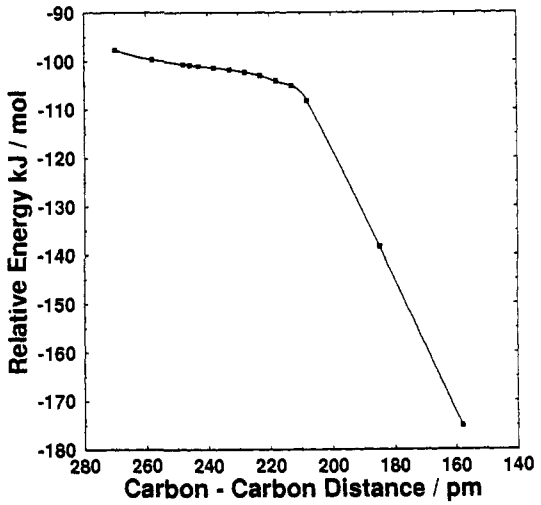

Figure 6. Energy profile of the ethylene insertion into the Ti–C bond of $Cp_2TiCH_3^+$, MP2-optimized geometries, basis A as described in section II.

This has in fact been demonstrated for Cl_3TiCH_3(dmpe),[33] where MP2 reproduces the neutron diffraction data[34] with deviations of less than 5 pm (for the rather weak Ti–P bond), roughly a factor of 4 smaller than for the SCF structure, vide infra.

It is appropriate, however, to check the performance of MP2 for the present cases by means of an SCF stability analysis which has been used before in this context.[12,33]

In a previous treatment of Cl_3TiCH_3(dmpe)[33] it was established that this system has one negative eigenvalue in the SCF triplet instability[26] matrix. We have demonstrated[33]—through the analysis of the UHF natural orbitals—that this instability is caused by the "left/right" correlation of the bonding/antibonding Ti–C σ bond pair. All systems investigated here show this instability. This deficiency of the SCF method is rectified by the double (i.e. by $\sigma^2 \rightarrow \sigma^{*2}$) replacements included in the MP2 method. The agreement of the computed structure with the experimental one obtained by neutron diffraction[34] was excellent (deviations of less than 2 pm and 2° for the geometrical parameters concerning Ti and the agostically distorted methyl group), which strongly supports our analysis that MP2 is an appropriate method in systems of that kind.

(33) Weiss, H.; Haase, F.; Ahlrichs, R. *Chem. Phys. Lett.* **1992**, *194*, 492.
(34) Dawoodi, Z.; Green, M. L. H.; Mtetwa, V. S. B.; Prout, K.; Schultz, A. J.; Williams, J. M.: Koetzle, T. F. *J. Chem. Soc., Dalton Trans.* **1986**, 1629.

Table 4. Comparison of Methods: Fully Optimized SCF, LDF, and MP2 Geometries of the Educt $Cp_2TiCH_3^+$[a]

	SCF (Figure 7)	LDF (Figure 9)	MP2 (Figure 8)
geometry parameter			
Ti11–C12	211	207	211
Ti11–H14	258	214	203
C12–H15, H16	109	110	111
C12–H14	109	114	115
C–C(Cp)	142	141–142	145–146
Ti11–center(Cp)	206/207	198/199	202/203
Ti11–C(Cp)	239–241	230–232	236–241
center(Cp)–Ti11–center(Cp)	141.3	137.7	138.2
Ti11–C12–H14	102.1	77.6	70.2
Ti11–C12–H13	114.4	123.4	125.1
Ti11–C12–H15	115.2	123.4	123.7
dihedral			
H21–C16–C1–H6	17.0	25.1	11.7
out-of-plane bend			
H15–Ti11–H13–C12	46.0	19.5	11.7

[a] Important bond lengths (pm) and angles (deg) for basis B (SCF and MP2) and DND as referenced in section II.

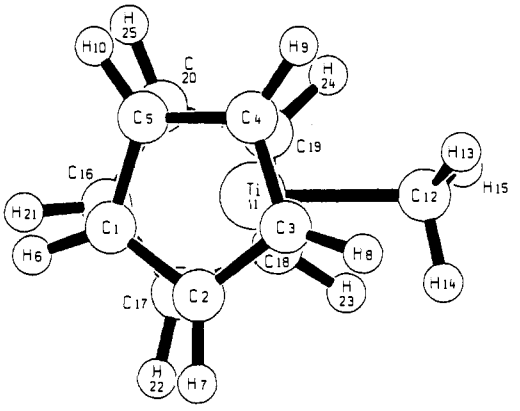

Figure 7. Optimized geometry of $Cp_2TiCH_3^+$ at the SCF level, basis B as described in section II. Important bond distances (pm) and angles (deg) are as follows: Ti11–C12, 211; Ti11–H14, 258; C12–H15, H16, 109; C12–H14, 109; C–C(Cp), 142; Ti11–center(Cp), 206/207; Ti11–C(Cp), 239–241; center(Cp)–Ti–center(Cp), 141.3; Ti11–C12–H14, 102.1; Ti11–C12–H13, 114.4; Ti11–C12–H15, 115.2; dihedral H21–C16–C1–H6, 17.0; out-of-plane bend H15–Ti11–H13–C12, 46.0.

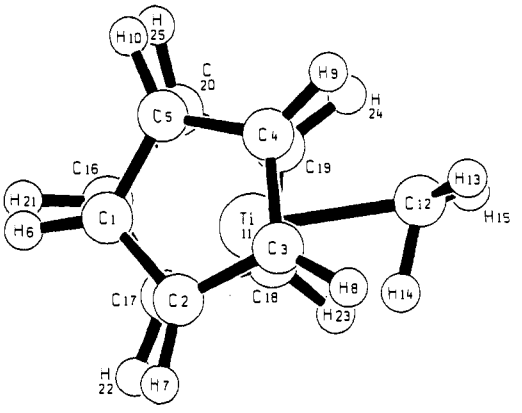

Figure 8. Optimized geometry of $Cp_2TiCH_3^+$ at the MP2 level, basis B as described in section II. Important bond distances (pm) and angles (deg) are as follows: Ti11–C12, 211; Ti11–H14, 203; Ti11–H15, H16, 111; C12–H14, 115; C–C(Cp), 145–146; Ti11–center(Cp), 202/203; Ti11–C(Cp), 235–239; center(Cp)–Ti11–center(Cp), 138.2; Ti11–C12–H14, 70.2; Ti11–C12–H13, 125.1; Ti11–C12–H15, 123.7; dihedral H21–C16–C1–H6, 11.7; out-of-plane bend H15–Ti11–H13–C12, 11.7.

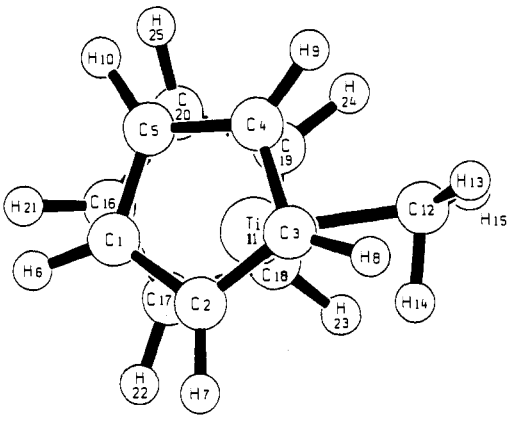

Figure 9. Optimized geometry of $Cp_2TiCH_3^+$ at the LDF level. Important bond distances (pm) and angles (deg) are as follows: Ti11–C12, 207; Ti11–H14, 214; C12–H15, H16, 110; C12–H14, 114; C–C(Cp), 141–142; Ti11–center(Cp), 198/199; Ti11–C(Cp), 230–232; center(Cp)–Ti–center(Cp), 137.7; Ti11–C12–H14, 77.6; Ti11–C12–H13, 123.4; Ti11–C12–H15, 123.4; dihedral H21–C16–C1–H6, 25.1; out-of-plane bend H15–Ti11–H13–C12, 19.5.

For the $Cp_2TiCH_3^+$–C_2H_4 system, we first checked whether there are significant changes in the eigenvalue spectrum of the singlet, triplet, and nonreal matrices during the ethylene insertion. These instability calculations were performed at the corresponding SCF equilibrium geometries with basis B. The results are collected in Table 2. The eigenvalue spectrum remains nearly unchanged over the entire reaction path. There are no negative or critically small eigenvalues in the singlet and the nonreal instability matrices. The triplet instability is of the same type as that in Cl_3TiCH_3-(dmpe) and therefore is corrected by the MP2 method in all probability. For the $Cl_2TiCH_3^+$–C_2H_4 system, this instability has first been described by Kawamura-Kuribayashi, Koga, and Morokuma.[12] We will compare their results and conclusions with ours in section V.

IV. The $Cp_2TiCH_3^+$–C_2H_4 System

The ideas of the Cossee–Arlman[7] (CA for short) mechanism have strongly influenced quantum chemical calculations on ethylene insertion published so far. According to the CA mechanism, the precoordinated monomer (π complex) and a four-membered transition state have been searched and found in semiempirical[11] and SCF[12] calculations.

As a start we performed SCF investigations of the $Cp_2TiCH_3^+$–C_2H_4 system. Using basis B, our results seemed to confirm the concepts of CA. We found local minima (proven to be local minima by calculations of the force constant matrices) for the π complex (Figure 3) and the γ-agostic product (Figure 4). By applying a saddle point searcher, we were able to locate a true transition state (Figure 5) with one and only one imaginary frequency at $i504$ cm^{-1}. The first doubts about the reliability of our SCF results came with single point MP2/SCF calculations (single point MP2 calculations at the SCF-optimized equilibrium geometries). The results of these energy calculations are collected in Table 1. On the MP2/SCF level, the SCF transition state is stabilized against the π complex by about 23 kJ/mol. Single point calculations with basis C confirmed this result which contradicts the CA mechanism.

We then performed MP2 geometry optimizations without any constraints to check the energetics of the ethylene insertion with a true Ziegler–Natta catalyst at the correlated equilibrium geometries. No orbitals were frozen and no symmetry was assumed. We used basis sets A, B, and, for the optimization of the educt, C. *The results are clear cut: we found no local minimum between the educt and the product. In particular, there is no precoordinated monomer on a correlated level. The potential energy surface is extremely flat as is demonstrated by the energy profile (Table 3) plotted in Figure 6.* We cannot rule out that a higher level treatment—which was not possible for us—leads to a different result, e.g. a local minimum for the π complex. Single point CCSD(T) calculations for $Cl_2TiCH_3^+$–C_2H_4 (section V) do in fact increase the activation energy (π complex vs transition state) from 10.7 kJ/mol (MP2) to 21.7

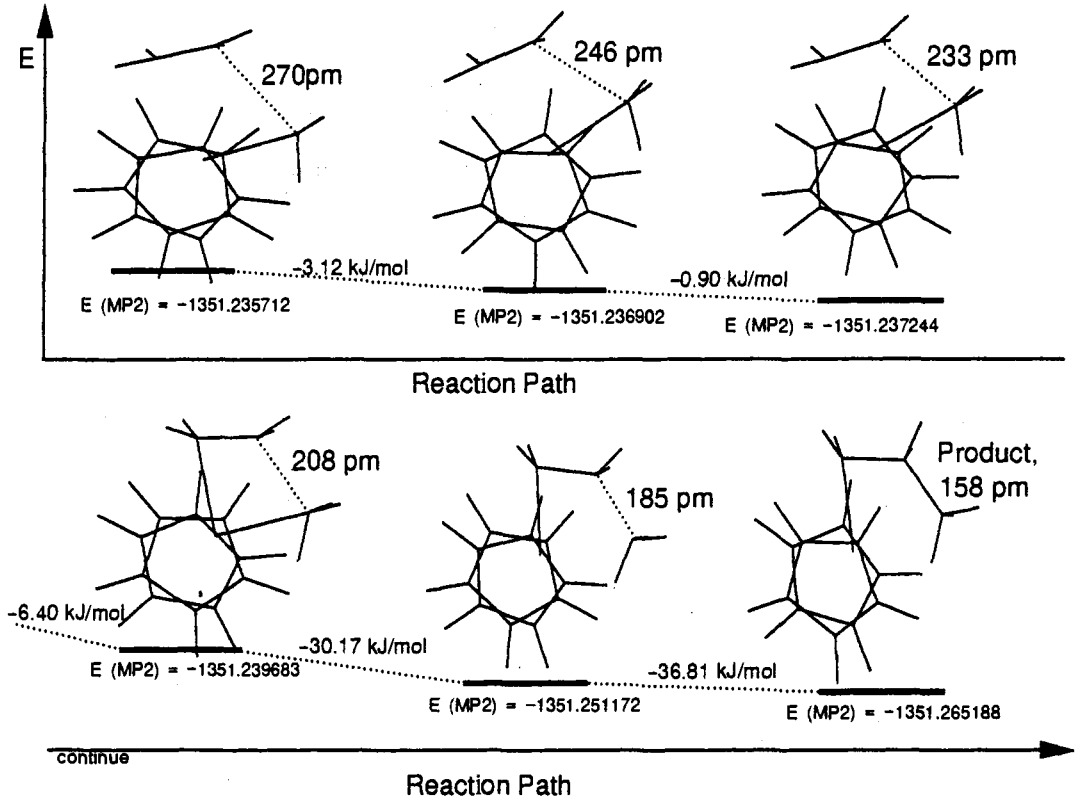

Figure 10. Reaction path of the ethylene insertion into the Ti–C bond of $Cp_2TiCH_3^+$, MP2 optimized geometries, basis A as described in section II.

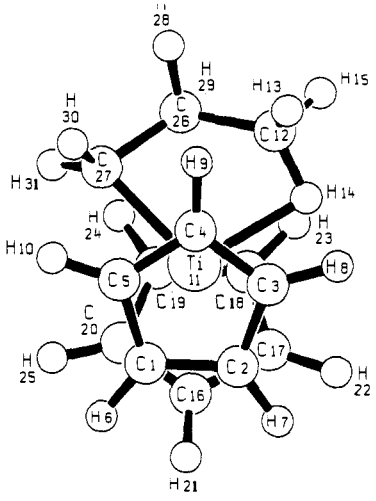

Figure 11. Optimized geometry of the γ-agostic propyl complex, the primary product of ethylene insertion into the Ti–C bond of $Cp_2TiCH_3^+$ at the LDF level. Important bond distances (pm) and angles (deg) are as follows: Ti11–C12, 239; Ti11–C27, 208; Ti11–H14, 198; C12–C26, 155; C27–C26, 155; C12–H14, 114; C12–H13, H15, 110; C27–H30, H31, 111; C–C(Cp), 141–142; Ti11–center(Cp), 201/202; Ti11–C(Cp), 231–238; center(Cp)–Ti–center(Cp), 134.2, Ti11–C12–H14, 55.7; Ti11–C27–C26, 82.1; C27–C26–C12, 123.3; C26–C12–H14, 121.0; C12–H14–Ti11, 95.8; H14–Ti11–C27, 102.7; out-of-plane bend H30–H31–Ti11–C27, 34.4; dihedral H21–C16–C1–H6, –44.7; dihedral C27–C26–C12–H14, 53.7.

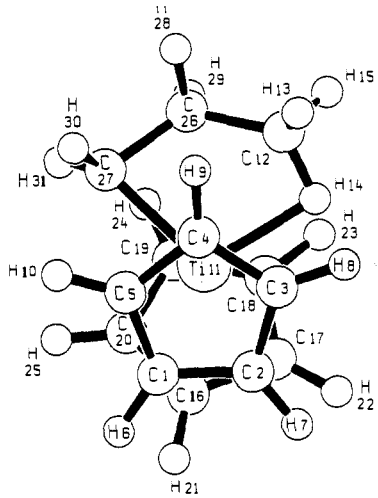

Figure 12. Optimized geometry of the γ-agostic propyl complex, the primary product of ethylene insertion into the Ti–C bond of $Cp_2TiCH_3^+$ at the MP2 level, basis B as described in section II. Important bond distances (pm) and angles (deg) are as follows: Ti11–C12, 238; Ti11–C27, 212; Ti11–H14, 197; C12–C26, 158; C27–C26, 158; C12–H14, 114; C12–H15, H16, 110; C27–H30, H31, 111; C–C(Cp), 144–145; Ti11–center(Cp), 204/204; Ti11–C(Cp), 239–241; center(Cp)–Ti–center(Cp), 132.8; Ti11–C12–H14, 55.5; Ti11–C27–C26, 79.6; C27–C26–C12, 125.8; C26–C12–H14, 121.8; C12–H14–Ti11, 95.9; H14–Ti11–C27, 105.3; out-of-plane bend H31–Ti11–H30–C27, 27.3; out-of-plane bend H30–H31–Ti11–C27, 28.8; dihedral H21–C16–C1–H6, –28.3; dihedral C27–C26–C12–H14, 47.6.

kJ/mol. A similar effect can be expected here which would lead to a barrier between 0 kJ/mol (since the MP2 surface is downhill) and 10 kJ/mol. A barrier of this magnitude would hardly be distinguishable from a strictly downhill potential as far as kinetics are concerned. By applying the LDF method, the same observations were made: LDF and MP2 give qualitatively the same results. We now discuss the structure and energetics in more detail.

(A) Structure of the Educt $Cp_2TiCH_3^+$. By employing basis sets A, B, and C for the SCF and MP2 optimizations, we found that the agreement is excellent with deviations of 1–2 pm and 1–2°. For reasons of consistency, we discuss the structures obtained with basis B. By comparing (Table 4) the structures obtained within the SCF method (Figure 7), the MP2 method (Figure 8), and the LDF method (Figure 9), the most remarkable result is that, on the correlated levels, the methyl group is heavily distorted through α-agostic interactions. Particularly noteworthy is that the "backside attack" of the C12–H14 σ bond upon the unsaturated metal center allows a quasiplanar conformation of the H atoms 13 and 15 (Figures 7–9) with the methyl carbon and the Ti center: the out-of-plane bend between the H15–C12 bond and the plane of Ti, H13, and C12 is reduced from 46° (SCF) to 12° (MP2). It is obvious that, during the insertion process, the repulsion between the approaching monomer and the methyl group (or the polymer chain in general) is strongly reduced by this quasiplanarity. This is the way the ethylene insertion is assisted by agostic interactions as proposed by Brookhart and Green. The Ti–C12 distance is 211 pm both for SCF and MP2. One would expect (as has been found for $Cl_3TiCH_3(dmpe)$[33]) that the inclusion of the σ/σ^* correlation on the MP2 level should lengthen the bond by roughly 3–4 pm. Obviously, this effect is compensated by agostic interactions as may be rationalized through the tautomeric structures $[Ti]—CH_3 \rightleftharpoons [Ti]H=CH_2$.

(B) π Complex and Transition State. The π complex does not exist on the MP2 or LDF level. On the SCF level (Figure 3), the binding energy of the olefinic monomer is only 22.3 kJ/mol (Table 1). The distance between Ti and the olefinic carbon atoms is roughly 300 pm, in agreement with previous semiempirical results.[11] It is noteworthy that neither the active catalyst nor the π-bound monomer differ significantly from their isolated equilibrium structures, which is in line with the small binding energy. The absence of a π complex is certainly not in disagreement with experimental facts.

The active catalyst **1** is so reactive that it is undetectable under normal spectroscopical conditions.[2,35] The recent detection[6] of a stabilized surrogate of **1** required sophisticated temperature-dependent multinuclear magnetic resonance techniques.[6] Regarding the structure of **1** as determined through our correlated calculations, this high reactivity is expected since the structure is reminiscent of that of a metallacarbene. The ethylene insertion is then rationalized by reference to a 2 + 2 addition which is symmetry allowed through the availability of d orbitals.[11,36,37] Activation energies of this type of reaction are known to be very low.

We have calculated (Figure 10) the reaction path of the insertion process with the MP2 method using basis A. As a reaction coordinate, we have chosen the distance R_r between the two carbon atoms C12 and C26 (see Figure 3 for labeling) that form the new bond. For a series of fixed C12–C26 distances, the molecule was completely relaxed. The energies as a function of the distance and the remaining gradients (giving the slope on the potential energy surface) are collected in Table 3. At 246 pm, the gradient dropped below the threshhold of 10^{-3} hartree/bohr (the default value in our program). Various attempts to locate a saddle point on the MP2 level with a saddle point searcher were futile. Therefore, we regard this area as a plateau on the extremely flat potential energy surface. Between R_r of 270 and 208 pm, the energy difference is about 8 kJ/mol! Nevertheless, MP2 and LDF provide the very same information. The structures of the educt and product are in good agreement and show the same essential features concerning the agostic interactions. This agreement is also reflected in the energetics: the reaction energy calculated on the MP2 level with basis B is –188.9 kJ/mol, and with the LDF method, –195.1 kJ/mol (Table 1), which will be further discussed below.

(35) Long, W. P. *J. Am. Chem. Soc.* **1959**, *81*, 5312.
(36) Upton, T. H. *J. Am. Chem. Soc.* **1984**, *106*, 1561.
(37) Steigerwald, M. L.; Goddard, W. A., III. *J. Am. Chem. Soc.* **1984**, *106*, 308.

Table 5. Comparison of Methods: Fully Optimized SCF, LDF, and MP2 Geometries of the Primary Insertion Product, the γ-Agostic $Cp_2TiC_3H_7^+$[a]

	SCF (Figure 4)	LDF (Figure 11)	MP2 (Figure 12)
Ti11–C12	360	239	238
Ti11–C27	214	208	212
Ti11–H14	318	198	197
C12–C26	153	155	158
C27–C26	154	155	158
C12–H14	110	114	114
C12–H15, H13	110	110	110
C27–H30, H31	109	111	111
C–C(Cp)	141–142	141–142	144–145
Till-center(Cp)	207/207	201/202	204/204
Ti11–C(Cp)	239–241	231–238	239–241
center(Cp)-Ti-center(Cp)	139.4	134.2	132.8
Ti11–C12–H14	59.0	55.7	55.5
Ti11–C27–C26	118.1	82.1	79.6
C27–C26–C12	114.1	123.3	125.8
C26–C12–H14	112.2	121.0	121.8
C12–H14–Ti11	103.8	95.8	95.9
H14–T11–C27 out-of-plane bend	62.1	102.7	105.3
H31–Ti11–H30–C27 dihedral	64.3	34.4	27.3
H21–C16–C1–H6	–41.5	–44.7	–28.3
C27–C26–C12–H14	62.3	53.7	47.6

[a] Important bond lengths (pm) and angles (deg) for basis B (SCF and MP2) and DND (LDF).

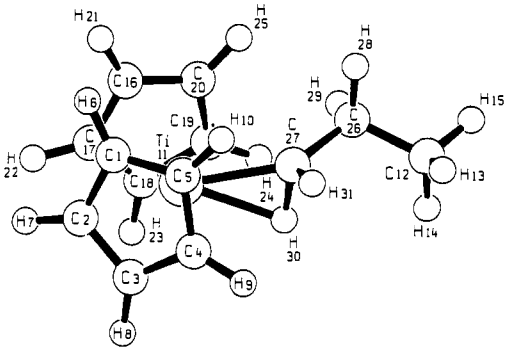

Figure 13. Optimized geometry of the α-agostic propyl complex at the LDF level, basis DND as referenced in section II. Important bond distances (pm) and angles (deg) are as follows: Ti11–C27, 208; Ti11–H30, 200; C12–C26, 151; C27–C26, 149; C27–H30, 116; C27–H31, 110; C12–H13, H14, H15, 110; C–C(Cp), 140–142; Ti11–center(Cp), 197/198; Ti11–C(Cp), 228–234; center(Cp)–Ti–center(Cp), 138.7; Ti11–C27–H30, 69.7; Ti11–C27–H31, 113.9; C26–C12–H13, 111.6; C26–C12–H14, 111.3; C26–C12–H14, 111.0; C27–C26–C12, 112.0; out-of-plane bend C26–Ti11–H31–C27, 11.1; dihedral H21–C16–C1–H6, 3.3; dihedral Ti11–C27–C26–C12, –146.1.

It is important to stress that the computed results described above do not contradict the experimental findings. The "activation energy" of the ethylene insertion is often identified with the polymerization propagation energy, which is experimentally determined to be roughly 30 kJ/mol,[38] but it has not been possible to assign this barrier to a specific reaction step. The present results imply that the barrier does not correspond to the insertion.

(C) The Products: α-, β-, and γ-Agostic $Cp_2TiC_3H_7^+$. The primary insertion product is the γ-agostic $Cp_2TiC_3H_7^+$ within all methods used in this work. LDF (Figure 11) and MP2 (Figure 12) again provide the same information (Table 5), whereas the SCF method (Figure 4) underestimates agostic interactions. This preponderance of γ-agostic primary products is predicted by the Brookhart–Green[8] (B–G) mechanism. According to this mechanism, the product isomerizes in a stepwise conversion via a β-agostic intermediate to the final α-agostic product. This

(38) Chien, J. C. W.; Razavi, A. *J. Polym. Sci., Part A: Polym. Chem.* **1988**, *26*, 2369.

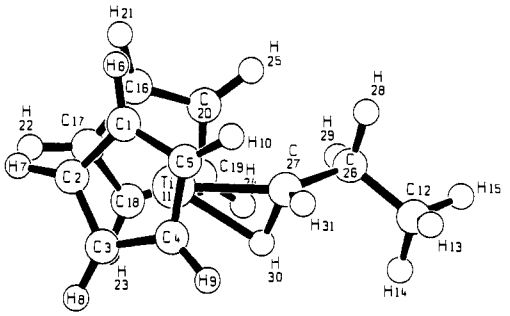

Figure 14. Optimized geometry of the α-agostic propyl complex at the MP2 level, basis B as described in section II. Important bond distances (pm) and angles (deg) are as follows: Ti11–C27, 213; Ti11–H30, 199; C12–C26, 154; C27–C26, 152; C27–H30, 117; C27–H31, 111; C12–H13, H14, H15, 111; C–C(Cp), 144–146; Ti11–center(Cp), 202/202; Ti11–C(Cp), 235–239; center(Cp)–Ti–center(Cp), 137.4; Ti11–C27–H30, 67.0; Ti11–C27–H31, 113.3; C26–C12–H13, 111.1; C26–C12–H14, 111.1; C26–C12–H15, 110.9; C27–C26–C12, 113.0; out-of-plane bend C26–Ti11–H31–C27, 9.5; dihedral H21–C16–C1–H6, –6.0; dihedral Ti11–C27–C26–C12, –143.7.

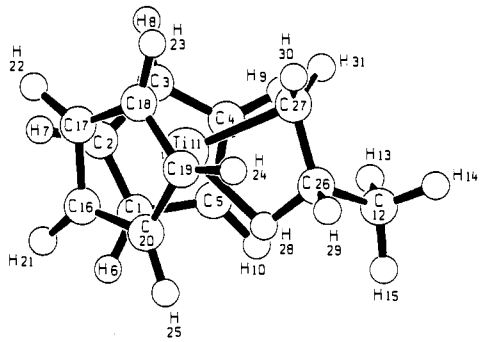

Figure 15. Optimized geometry of the β-agostic propyl complex at the LDF level, basis DND as referenced in section II. Important bond distances (pm) and angles (deg) are as follows: Ti11–C27, 213; Ti11–C26, 242; Ti11–H30, 190; C12–C26, 151; C27–C26, 148; C26–H28, 119; C26–H29, 111; C27–H29, H30, H31, 110; C12–H13, H14, H15, 111; C–C(Cp), 141–142; Ti11–center(Cp), 199/202; Ti11–C(Cp), 230–234; center(Cp)–Ti–center(Cp), 142.0; Ti11–C27–C26, 82.1; Ti11–C27–H31, 113.9; C26–C12–H13, 111.6; C26–C12–H14, 111.3; C26–C12–H14, 111.0; C27–C26–C12, 112.0; out-of-plane bend H31–Ti11–H30–C27, 41.6; dihedral H21–C16–C1–H6, –30.7, dihedral Ti11–C27–C26–H28, 1.7; dihedral Ti11–C27–C26–C12, 120.7.

α-agostic product is assumed to assist the carbon–carbon bond forming step through steric effects since it would allow the other atoms on the α-carbon atom to more readily move away from an approaching carbon of the olefin. By following these plausible arguments, we optimized the structures of the α- (LDF, Figure 13; MP2, Figure 14), β- (LDF, Figure 15; MP2, Figure 16), and γ-agostic (LDF, Figure 11; MP2, Figure 12) $Cp_2TiC_3H_7^+$. In the crucial geometrical parameters, the geometries of the educt and α-agostic products agree perfectly within LDF and MP2, respectively: the Ti–C bond lengths are almost identical and, most important, the α-agostic C has a nearly planar environment on the active side of the Ti center. Thus, the Ti–C bond again shows the carbenoid character found in the educt and there is no reason to expect that the insertion of another monomer into the growing alkyl chain should be less easy than the initial one. Therefore, from the geometrical aspects, the results strongly support the B–G mechanism.

The energetics are less clear-cut.[39] On the LDF level, the γ-agostic product is only 1.2 kJ/mol more stable than the α-agostic

(39) As the CCSD(T) calculations have shown (section V), the MP2 energetics are reliable. Thus we regard the LDF results simply as estimates for the more accurate MP2 energies. We are aware of the problems in determining energies with nongradient corrected density functionals.[40] For the systems considered here, we found that the LDF energies generally agree with the MP2 results—with the exception of the α-agostic product.

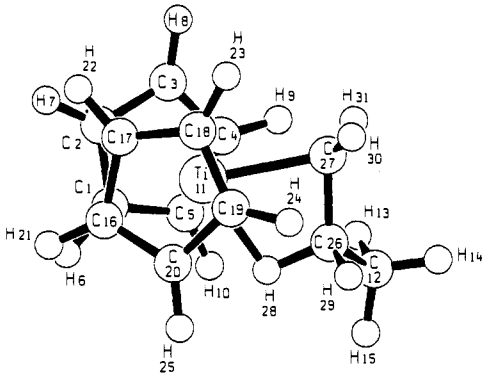

Figure 16. Optimized geometry of the β-agostic propyl complex at the MP2 level, basis B as described in section II. Important bond distances (pm) and angles (deg) are as follows: Ti11–C27, 217; Ti11–C26, 243; Ti11–H30, 193; C12–C26, 153; C27–C26, 151; C26–H28, 118; C26–H29, 111; C27–H29, H30, H31, 110; C12–H13, H14, H15, 111; C–C(Cp), 144–145; Ti11–center(Cp), 202/202; Ti11–C(Cp), 234–239; center(Cp)–Ti–center(Cp), 137.0; Ti11–C27–C26, 80.8; Ti11–C27–H31, 119.3; C26–C12–H13, 111.6; C26–C12–H14, 108.8; C26–C12–H15, 112.0; C27–C26–C12, 115.8; out-of-plane bend H31–Ti11–H30–C27, 37.72; dihedral H21–C16–C1–H6, –21.8; dihedral Ti11–C27–C26–H28, 5.0; dihedral Ti11–C27–C26–C12, 124.0.

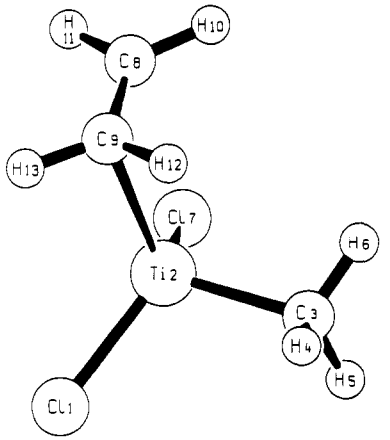

Figure 17. Optimized geometry of the precoordinated ethylene on $Cl_2TiCH_3^+$ at the MP2 level, basis A as described in section II. Important bond distances (pm) and angles (deg) are as follows: Ti2–C3, 199; Ti2–Cl1, 212; Ti2–Cl7, 213; C8–C9, 137; C8–C3, 389; C8–Ti2, 273; C9–Ti2, 231; C3–H4, 112; C3–H5, 112; C3–H6, 112; Ti2–C3–H5, 112.6; Ti2–C3–H6, 105.6; Cl1–Ti2–Cl7, 115.6; H6–C3–H4, 111.0; H6–C3–H5, 109.4; H4–C3–Ti2, 108.5; torsion C8–C9–Ti2–C3, 102.7; out-of-plane bend H6–Ti2–H4–C3, 57.3; out-of-plane bend H13–H12–C8–C9, 9.7; out-of-plane bend H10–H11–C9–C8, 1.1.

one, but on the MP2 level, this stabilization energy increases to 46.7 kJ/mol. This means that, on the LDF level, the isomerization of the initially formed γ-product into the α-product is very likely at room temperatures. The LDF calculations seem to confirm the B–G mechanism. Against that, the isomerization energy found on the MP2 level is appreciable and it is questionable whether the isomerization takes place; however, it is not excluded by our results.

On the other hand, one should ask whether an isomerization is really necessary. On the basis of our geometries, it appears possible that the insertion of another monomer occurs with ease both into the α- and γ-agostic products. Both isomers have comparable bond lengths, and the out-of-plane bends on the α-carbon atoms (approximately 10° for the α-product and 30° for the γ-agostic product), indicate carbenoid character for the Ti–C bonds of both isomers. Answering this question is not possible without investigating the ethylene insertion into the α- and γ-agostic $Cp_2TiC_3H_7^+$.

The third relevant isomer of $Cp_2TiC_3H_7^+$ is the β-agostic species. We found that this is the most stable isomer. Its energies of stabilization against the γ-agostic $Cp_2TiC_3H_7^+$ are 16.5 kJ/mol (LDF) and 9.0 kJ/mol (MP2). The β-agostic isomer has the least carbenoid character. This is documented by the LDF Ti–C bond lengths (α- and γ, 208 pm; β, 213) and the out-of-plane bends at the α-carbon atom (9.5° for the α-agostic complex, 34.4° for the γ-agostic complex, and 41.6° for the β-agostic $Cp_2TiC_3H_7^+$) and by the fact that it is the most stable species. We agree with Brookhart and Green and consider the β-agostic isomer to be an intermediate in the stepwise conversion of the primary γ-agostic insertion product to the α-agostic species.

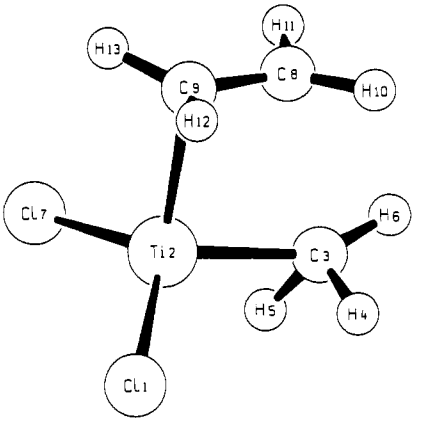

Figure 18. MP2 transition state of the ethylene insertion into the Ti–C bond of $Cl_2TiCH_3^+$ basis A as described in section II. Important bond distances (pm) and angles (deg) are as follows: Ti2–C3, 199; Ti2–Cl1, 214; Ti2–Cl7, 213; C8–C9, 139; C8–C3, 239; C8–Ti2, 253; C9–Ti2, 218; C3–H4, 112; C3–H5, 115; C3–H6, 112; Ti2–C3–H5, 76.7; Cl1–Ti2–Cl7, 120.2; H6–C3–H4, 109.9; H6–C3–H5, 105.4; H4–C3–Ti2, 95.5; Ti2–C3–H6, 151.45; dihedral C8–C9–Ti2–C3, 13.5; out-of-plane bend H6–Ti2–H4–C3, 12.4; out-of-plane bend H13–H12–C8–C9, 15.1; out-of-plane bend H10–H11–C9–C8, 11.7.

Table 6. Comparison of Methods: Energies on Various Levels of Theory for the System $Cl_2TiCH_3^+$–C_2H_4 at the MP2 Equilibrium Geometries[a]

	$Cl_2TiCH_3^+ + C_2H_4$ (Figure 19)	π complex (Figure 17)	TS[b] (Figure 18)	γ-product (Figure 21)	activation energy
SCF	0	–147.1	–95.6	–170.9	51.5
LDF[c]	0	–179.3	–170.8	–266.5	8.5
MP2	0	–175.9	–165.2	–242.2	10.7
	(0)[d]	(–102.0)[d]	(–94.7)[d]	(–162.5)[d]	(7.3)[d]
CCSD	0	–154.9	–132.4	–215.8	22.5
CCSD(T)	0	–161.9	–140.2	–214.3	21.7

[a] Basis A was used throughout. The energies are given relative to $Cl_2TiCH_3^+$ and C_2H_4 in kJ/mol. [b] Transition state. [c] Energies at the LDF equilibrium geometries. [d] Values in parentheses give the relative energies for the system $Cl_2TiC_3H_7^+$–C_2H_4, i.e. the second insertion step. The relative energies during the insertion (i.e. after the formation of the π complex) remain nearly unchanged for the first and the second insertion steps (see section V).

V. The $Cl_2TiCH_3^+$–C_2H_4 System

Finally we discuss results of the MP2 calculations performed on the $Cl_2TiCH_3^+$–C_2H_4 system since it has often[10–12] served as a model for $Cp_2TiCH_3^+$–C_2H_4 in theoretical investigations. The present investigations reveal some differences, however, which essentially concern the agostic effects.

We found again the triplet instabilities typical of these systems. We cannot confirm the collapse of the SCF wave function due to this triplet instability as described in a recent paper by Kawamura-Kuribayashi et al.[12] These authors performed single point MP2 and UMP2 (unrestricted MP2) calculations at the

(40) Ziegler, T. *NATO ASI Ser., Ser. C* (Energ. Organomet. Species) **1992**, *367*, 357.

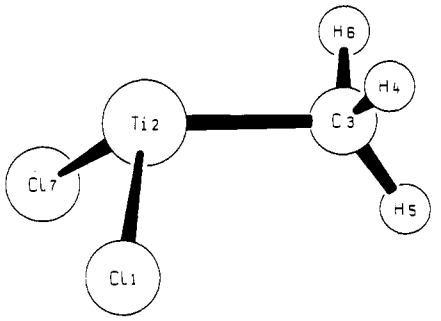

Figure 19. Optimized geometry of $Cl_2TiCH_3^+$ at the MP2 level, basis A as described in section II. Important bond distances (pm) and angles (deg) are as follows: Ti2–C3, 196; Ti2–Cl1, 210; Ti2–Cl7, 210; C3–H4, 112; C3–H5, 111; C3–H6, 112; Ti2–H4, 243; Ti2–H5, 277; Ti2–H6, 242; Ti2–C3–H4, 100.4; Ti2–C3–H5, 126.7; Ti2–C3–H6, 99.4; Cl1–Ti2–C3, 105.5; Cl1–Ti2–C7, 109.8; out-of-plane bend H4–H6–Ti2–C3, 65.3.

SCF-optimized geometries. For the MP2 energy of the product, they obtained an unrealistic stabilization of 1600 kJ/mol relative to the educts $Cl_2TiCH_3^+$ and C_2H_4. They concluded that UMP2 calculations are necessary to eliminate the effects of the triplet instability and found a more realistic stabilization energy of 237 kJ/mol with the double-projected UMP2 method. In our MP2 optimizations of the product, we could not observe this breakdown of the restricted wave function. We found a stabilization energy of 242 kJ/mol on the MP2 level (instead of 1600 kJ/mol), which compares well with the double-projected UMP2 result of Kawamura-Kuribayashi et al. We have no explanation for their MP2 results.

On the MP2 level, we found a precoordinated monomer (π complex, Figure 17) and a transition state (Figure 18). The quality of the MP2 energetics has been checked through single point CCSD(T) calculations at the MP2 equilibrium geometries for this system. The energies are collected in Table 6. A comparison of MP2 and CCSD(T) shows the typical behavior: MP2 slightly overestimates the correlation energy but is relatively reliable. The reaction energy for the monomer insertion is reduced from 242 kJ/mol (MP2) to 214 kJ/mol on the CCSD(T) level. The SCF result is 171 kJ/mol. Even the CCSD(T) reaction energy is considerably larger than expected: the energy for the ethylene insertion is known to be 96 kJ/mol. We offer the following explanation for this apparent discrepency. $Cl_2TiC_3H_7^+$ is stabilized, as compared to $Cl_2TiCH_3^+$, by the larger polarizability of the propyl group. Additional MP2 optimizations for the insertion of a second ethylene did in fact result in a reaction energy of only 162.5 kJ/mol as compared to 242.2 kJ/mol for the first insertion. This however hardly affects the actual insertion: the MP2 energy difference between the π complex, which is a local minimum even for the second insertion step, and the γ-agostic product changes only from 66.3 kJ/mol for the first insertion to 60.5 kJ/mol for the second insertion. This reveals that, although the energy for the first insertion step is too high, $Cl_2TiCH_3^+$ is an appropriate model.

The activation energy is 10.7 kJ/mol (7.3 kJ/mol for the second insertion) on the MP2 level and 21.7 kJ/mol on the CCSD(T) level. The SCF method (51.5 kJ/mol) clearly overestimates the activation energy. Thus both correlated methods show that the insertion is an easy but not spontaneous process for this system.

Table 7. Geometry Parameters of the Ethylene Insertion in the $Cl_2TiCH_3^+$–C_2H_4 System on the MP2 Level of Theory, Basis A[a]

	$Cl_2TiCH_3^+$ (Figure 19)	π complex (Figure 17)	TS[b] (Figure 18)	γ-product (Figure 21)
Ti2–C3	196	199	199	217
Ti2–C8		273	253	236
Ti2–C9		231	218	197
C8–C9		137	139	156
Ti2–Cl1	210	212	214	213
Ti2–Cl7	210	213	213	212
C3–H4	112	112	112	113
C3–H5	111	112	115	113
C3–H6	112	112	112	111
Cl1–Ti2–Cl7	109.8	115.6	120.2	116.5
Ti2–C3–H4	100.4	108.5	95.5	77.7
Ti2–C3–H5	126.7	112.6	76.7	73.6
Ti2–C3–H6	99.4	105.6	151.5	174.5
out-of-plane bend				
H6–Ti2–H4–C3	65.3	57.3	12.4	–5.5
dihedral				
C8–C9–Ti2–C3		102.7	13.5	7.2

[a] Important geometry parameters are given in pm and deg. [b] Transition state.

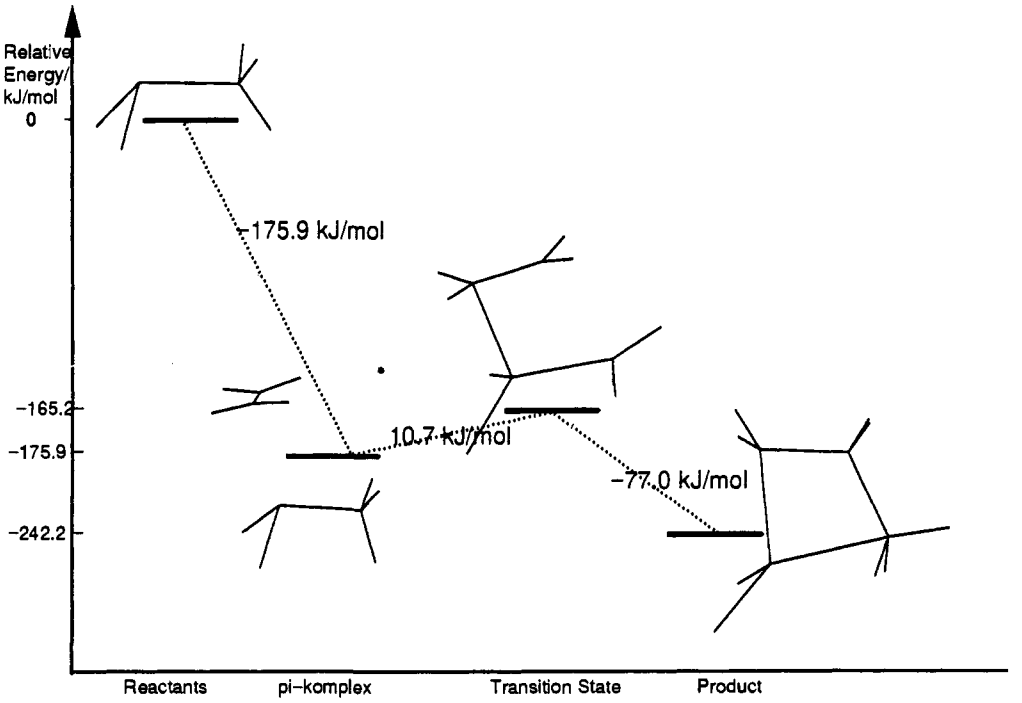

Figure 20. Energy profile of the ethylene insertion into the Ti–C bond of $Cl_2TiCH_3^+$, MP2 optimized geometries, basis A as described in section II.

Currently it is impossible for us for technical reasons to perform CCSD(T) calculations on the $Cp_2TiCH_3^+$–C_2H_4 system. Nevertheless, the MP2 calculations presented in the previous section win credibility since the CCSD(T) calculations clearly show that the systems investigated here are "good MP2" cases. They show that the triplet instability does not influence the quality of the MP2 calculations.

Important geometrical parameters are presented in Table 7. By comparing the structures of $Cl_2TiCH_3^+$ (Figure 19) and $Cp_2TiCH_3^+$ (Figure 8), it is obvious why the insertion is not spontaneous in the $Cl_2TiCH_3^+$–C_2H_4 system. For the $Cp_2TiCH_3^+$, there is a backside attack of the α-C–H bond upon the unsaturated metal center. This leads to the carbenoid character of the Ti–C bond and thus to the spontaneous insertion described above. In $Cl_2TiCH_3^+$, agostic interactions do not play a role. The approaching monomer sees a nearly undistorted methyl group with an out-of-plane bend between H4–H6–Ti2–C3 (see Figure 19 for labeling) of 65.3° (to compare, this out-of-plane bend was 11.7° for $Cp_2TiCH_3^+$). The resulting massive steric repulsion makes a spontaneous insertion energetically unfavorable and leads to a precoordinated monomer with a dihedral angle between the Ti–C bond and the C=C bond of the approaching monomer of 103°. One might argue that the reason why no bound π complex is obtained in the Cp case (but is obtained in the Cl_2 system) is that the small chloride ligands lead to much less steric repulsion than the Cp ligands. However, the Cp ligands are moved very easily to minimize repulsion. Thus, on the SCF level, there exists a bound π complex for the Cp case. The essential geometrical difference between the SCF and MP2 geometries is the agostically distorted methyl group. Thus we prefer a rationalization for the different behavior based on agostic effects.

In the transition state (Figure 18), the methyl group of the catalyst is distorted with the effect that now the out-of-plane H4–H6–Ti2–C3 is 12.3° as it is in the $Cp_2TiCH_3^+$ equilibrium geometry. The activation energy is 10.7 kJ/mol, which is consistent with previous results obtained by noncorrelated geometries. This is the main difference between the $Cp_2TiCH_3^+$ system and $Cl_2TiCH_3^+$–C_2H_4: $Cp_2TiCH_3^+$ with its carbenoid Ti–C bond allows the direct insertion, whereas the monomer suffers from steric repulsion through the methyl group in $Cl_2TiCH_3^+$. The insertion is nevertheless an easy step even in the $Cl_2TiCH_3^+$–C_2H_4 system, as can be seen from the energy profile plotted in Figure 20.

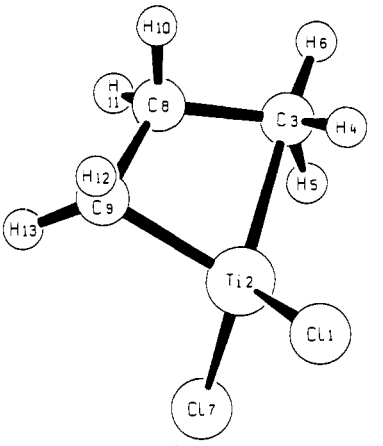

Figure 21. Optimized geometry of the γ-agostic propyl complex, the primary ethylene insertion product into the Ti–C bond of $Cl_2TiCH_3^+$ at the MP2 level, basis A as described in section II. Important bond distances (pm) and angles (deg) are as follows: C9–Ti2, 197; Ti2–C3, 217; Ti2–Cl1, 213; Ti2–Cl7, 212; C8–C9, 156; C8–C3, 159; C8–Ti2, 236; C3–H4, 113; C3–H5, 113; C3–H6, 111; C9–H12, 111; C9–H13, 111; Ti2–C3–H5, 73.6; Ti2–C3–H4, 77.7; Ti2–C3–H6, 174.5; Cl1–Ti2–Cl7, 116.5; Cl1–Ti2–C9, 110.1; Cl1–Ti2–C3, 118.2; Ti2–C9–C8, 83.1; C9–C8–C3, 118.0; C8–C3–Ti2, 76.2; C3–Ti2–C9, 81.4; dihedral C9–C8–C3–Ti2, 10.3; dihedral C8–C9–Ti2–C3, 7.2; out-of-plane bend H6–C8–C9–Ti2, 6.3; out-of-plane bend H6–Ti2–H4–C3, –5.5.

The primary insertion product is again the γ-agostic propyl complex (Figure 21). This time, however, there do not exist isomers with α- or β-agostic interactions on the MP2 level. This is another reason why we do not regard the $Cl_2TiCH_3^+$–C_2H_4 system as a quantitatively correct model for the Ziegler–Natta catalysis.

Acknowledgment. The authors thank Jürgen Gauss and Christian Huber for helpful comments concerning the CCSD(T) calculations. Computer time provided by Prof. Dr. D. Fenske and G. Baum is gratefully acknowledged. This work has been supported by the "Fonds der Chemischen Industrie".